Atmospheric
Chemistry
and Physics
Discussions

1 **Measurement report: Long emission-wavelength chromophores dominate the light absorption**

2 **of brown carbon in Aerosols over Bangkok: impact from biomass burning**

3 Jiao Tang[1,2,3], Jiaqi Wang[1,2,3,7], Guangcai Zhong[1,2,3], Hongxing Jiang[1,2,3,7], Yangzhi Mo[1,2,3], Bolong

4 Zhang[1,2,3,7], Xiaofei Geng[1,2,3,7], Yingjun Chen[4], Jianhui Tang[5], Congguo Tian[5], Surat Bualert[6], Jun

5 Li[1,2,3], Gan Zhang[1,2,3]

6 [1]State Key Laboratory of Organic Geochemistry and Guangdong Key Laboratory of Environmental

7 Protection and Resources Utilization, Guangzhou Institute of Geochemistry, Chinese Academy of

8 Sciences, Guangzhou 510640, China

9 [2]CAS Center for Excellence in Deep Earth Science, Guangzhou, 510640, China

10 [3]Joint Laboratory of the Guangdong-Hong Kong-Macao Greater Bay Area for the Environment,

11 Guangzhou Institute of Geochemistry, Chinese Academy of Sciences, Guangzhou 510640, China

12 [4]Department of Environmental Science and Engineering, Fudan University, Shanghai 200092, P.R.

13 China

14 [5]Key Laboratory of Coastal Environmental Processes and Ecological Remediation, Yantai Institute of

15 Coastal Zone Research, Chinese Academy of Sciences, Yantai 264003, China

16 [6]Faculty of Environment, Kasetsart University, Bangkok, 10900, Thailand

17 [7]University of Chinese Academy of Sciences, Beijing 100049, China

18

19 **Correspondence:** Guangcai Zhong (gczhong@gig.ac.cn)

20

21 **Abstract:** Chromophores represent an important portion of light-absorbing species, i.e. brown carbon.

22 Yet knowledge on what and how chromophores contribute to aerosol light absorption is still sparse. To

23 address this problem, we examined soluble independent chromophores in a set of year-round aerosol

24 samples from Bangkok. The water-soluble chromophores identified via excitation-emission matrix

25 (EEM) spectroscopy and follow-up parallel factor analysis could be mainly assigned as humic-like

26 substances and protein-like substances, which differed in their EEM pattern from that of the methanol-

27 soluble fraction. The emission wavelength of chromophores in environmental samples tended to

28 increase compared with that of the primary combustion emission, which could be attributed to

29 secondary formation or the aging process. Fluorescent indices inferred that these light-absorbing

30 chromophores were not significantly humified and comprised a mixture of organic matter of terrestrial

31 and microbial origin, while these inferences exhibited a refutation with primary biomass burning and

32 coal combustion results. A multiple linear regression analysis revealed that larger chromophores that

33 were oxygen-rich and highly aromatic with high molecular weights, were the key contributors of light

34 absorption, preferably at longer emission wavelength ($\lambda_{max} > 500$ nm). Positive matrix factorization

35 analysis further suggested that up to 60% of these responsible chromophores originated from biomass

36 burning emissions.

37

1. Introduction

Atmospheric aerosols play a substantial role in climate change through radiative forcing (Alexander et al., 2008). Carbonaceous aerosols mainly include organic carbon (OC) and elemental carbon (EC). Brown carbon (BrC) is a specific type of OC that absorbs radiation efficiently in the near-ultraviolet and visible (UV-vis) range (Laskin et al., 2015;Kirchstetter et al., 2004) and may contribute 15% or more of total light absorption over the UV-vis spectrum (Kirchstetter and Thatcher, 2012;Liu et al., 2013). This fraction can significantly affect atmospheric chemistry, air quality, and climate change (Marrero-Ortiz et al., 2018;Laskin et al., 2015). Forest fires, residential heating by wood and coal, biogenic release, and secondary formation contribute to BrC in the atmosphere (Laskin et al., 2015). Many studies have indicated that the optical properties of BrC may significantly evolve as a result of atmospheric processes such as oxidation (Fan et al., 2020), solar irradiation (Wong et al., 2017), and relative humidity (Kasthuriarachchi et al., 2020). These factors cause variability in the chemical compositions and levels of BrC across source regions and receptors, resulting in a high degree of uncertainty regarding the effects of BrC (Dasari et al., 2019;Xie et al., 2019).

Light absorption of BrC is associated with its molecular composition and chemical structure (Song et al., 2019;Lin et al., 2018;Mo et al., 2018;Jiang et al., 2020). Detailed structural characterization of BrC compounds is essential to understand their sources and chemical processes in the atmosphere. High-resolution mass spectrometry (HRMS) is a powerful tool for molecular-level chemical analysis of organic aerosols (Laskin et al., 2018). Combinations of offline high-performance liquid chromatography (HPLC), a photodiode array detector, and HRMS allow the chemical characterization of aerosols specific to BrC (Lin et al., 2018;Lin et al., 2016;Lin et al., 2015;Lin et al., 2017). With these combination approaches, nitroaromatics, aromatic acids, phenols, polycyclic aromatic hydrocarbons and their derivatives are basically identified as BrC chromophores (Wang et al., 2020b;Yan et al., 2020). However, it should be noted that it is difficult to ionize some organic compounds for detection using HRMS, and even for those that can be detected, HRMS can only provide possible molecular structures based on empirical deduction (Song et al., 2018;Lin et al., 2015). The isomeric complexity of natural organic matter may have exceeded achievable one-dimensional chromatographic resolution (Hawkes et al., 2018), and therefore, the majority of components in the BrC mixture remain undetermined.

Excitation-emission matrix (EEM) fluorescence spectroscopy detects bulk chromophores in a solution (Chen et al., 2016). Chromophores can be revealed by EEM with information on their chemical structures associated with molecular weight, aromatic rings, conjugated systems, etc (Wu et al., 2003). For example, a redshift in emission spectral maxima can be caused by an increase in the

71   number of aromatic rings condensed in a straight chain, conjugated double bonds, or formational

72   changes that permit vibrational energy losses of the promoted electrons (Wu et al., 2003). A significant

73   Stokes shift with emission wavelength can be observed in aged secondary organic aerosols (SOA)

74   using EEM spectroscopy (Lee et al., 2013). Parallel factor (PARAFAC) analysis has been widely used

75   to decompose the EEM spectral signature into independent underlying components (Han et al.,

76   2020;Yue et al., 2019;Wu et al., 2019;Chen et al., 2019b), adding valuable information to absorbance-

77   based measurements (Yan and Kim, 2017). This technique helps to categorize groups of similar

78   fluorophores or chromophores or similar optical properties, thereby allowing a better understanding of

79   the chemical properties of BrC. There is evidence that BrC absorption is closely correlated with

80   chromophores (Huo et al., 2018). However, the intrinsic relationship between chromophores and BrC

81   absorption has not been explored.

82   Southeast Asia is subject to intensive regional biomass burning, the emissions from which may

83   contribute to atmospheric brown clouds (Ramanathan et al., 2007;Laskin et al., 2015). The contribution

84   of biomass burning to aerosol optical depth was evaluated to be more than 56% over this region (Huang

85   et al., 2013). Despite many studies focused on the characterization of atmospheric black carbon (BC)

86   (See et al., 2006;Fujii et al., 2014;Permadi et al., 2018), studies on BrC in the region are still limited.

87   A recent study in Singapore indicated that water-soluble OC (WSOC) exhibited strong wavelength

88   dependence and even higher values of BrC absorption than those from Korea, India, China, and Nepal

89   (Adam et al., 2020), indicating abundant water-soluble BrC in the air over Southeast Asia.

90   This study was performed to explore the relationships between EEM chromophores and BrC light

91   absorption in soluble aerosol organic matter. A set of year-round aerosol samples from Bangkok,

92   Thailand, was analyzed. Water-soluble and methanol-soluble BrC in the aerosol samples were

93   characterized by EEM followed by statistical analyses to retrieve information on the contributions of

94   fluorescent chromophores to BrC light absorption, as well as their emission sources. This study

95   provides a comprehensive dataset on seasonal variability in the light absorption properties, sources,

96   and chemical components of BrC, which may be useful for improving further modeling and field

97   observation.

98   **2.   Experiment**

99   **2.1. Sample Collection and Extraction.**

100   Eighty-five total suspended particulate (TSP) samples were collected on the roof (57 m above

101   ground level) of the Faculty of Environment, Kasetsart University (100°57′ E and 13°85′ N) in

102   Bangkok, Thailand (Fig. S1). Detailed information about the sampling site is presented elsewhere

103   (Wang et al., 2020a). Sampling was performed from January 18, 2016 to January 28, 2017, and the

104   sampling period was divided into four seasons: the pre-hot season (January 18–February 28, 2016),

105   hot season (March 2–May 30, 2016), monsoon (June 2–October 30, 2016), and cool season (November

106   1, 2016–January 28, 2017). Table S1 lists the average meteorological data in the four seasons.

107   Generally, during the sampling period, the hot season was characterized by high temperatures and wind

108   speeds, and the monsoon season by high humidity. TSP samples were collected over 24 h using a high-

109   volume (0.3 m^3 min^{-1}) sampler with quartz-fiber filters (QFFs, prebaked for 6 h at 450 °C). All samples

110   and field blanks were stored under dark conditions at –20 °C until analysis.

111   WSOC was prepared by ultrasonication extraction of filter punches with ultra-pure deionized

112   water ($\Omega > 18.2$). The methanol-soluble OC (MSOC) fraction was then obtained by extracting the

113   freeze-dried residue on GFFs with HPLC-grade methanol, which is used for water-insoluble fractions

114   (Chen and Bond, 2010). The extract solutions were passed through 0.22-μm PTFE filters and subjected

115   to follow-up UV-vis absorption and fluorescence spectral analysis. The mass concentrations of WSOC

116   and MSOC were measured, and the method are shown in the Supplement.

2.2. Absorption Spectra and Fluorescence Spectra.

117

118   The extract solutions were placed in quartz cells with a path-length of 1 cm and subjected to

119   analysis using an fluorometer (Aqualog; Horiba Scientific, USA). Absorption spectra and EEM spectra

120   were obtained simultaneously using this instrument. The contribution of solvents was subtracted from

121   the extract spectra. UV-vis absorption spectra were scanned in the range of 239 to 800 nm with a step

122   size of 3 nm. The Fluorescence spectra were recorded with emission wavelength (Em) ranging from

123   247.01 to 825.03 nm and excitation wavelength (Ex) ranging from 239 to 800 nm. The wavelength

124   increments of the scans for Em and Ex were 4.66 and 3 nm, respectively. The calculation of optical

125   parameters and the relative contributions of BrC to total aerosol light absorption are presented in the

126   Supplement.

2.3. Factor analysis

127

128   In this study, we built a PARAFAC model, based on 85 TSP sample fluorescence (samples × Ex

129   × Em: 85 × 188 × 125, 85-model). Original EEM spectra were corrected and decomposed via

130   PARAFAC analysis with reference to earlier methods using drEEM toolbox version 2.0 with MATLAB

131   software (http://models.life.ku.dk/drEEM, last access: June 2014) (Murphy et al., 2013;Andersson and

132   Bro, 2000). The absorbance, all below 1 at 239 nm, was deemed suitable for correcting the EEM

133   spectra for inner filter effects (IFEs) (Luciani et al., 2009;Gu and Kenny, 2009;Fu et al., 2015), and the

134   sample EEM spectra, and blanks were normalized relative to the Raman peak area of ultrapure

135   deionized water collected on the same day to correct fluorescence in Raman Units (RU) (Murphy et

Atmospheric
Chemistry
and Physics
Discussions

136   al., 2013;Murphy et al., 2010). Spectra with Em > 580 nm and Ex < 250 nm were removed to eliminate

137   noisy data. The non-negativity constraint is necessary to obtain reasonable spectra, and signals of first-

138   order Rayleigh, Raman, and second-order Rayleigh scattering in the EEM spectra were removed using

139   the interpolation method (Bahram et al., 2006). The two- to nine-component PARAFAC model was

140   explored, within the context of spectral loading, core consistency, and residual analysis (Figs. S2–S5).

141   Finally, seven and six components were identified in the WSOC and MSOC fractions, which explained

142   99.89% and 99.76% of the variance, respectively. Both the seven- and six-component PARAFAC

143   solutions passed the split-half analysis with the split style of "$S_4C_6T_3$", and residuals were examined

144   to ensure that there was no systematic variation. The parameters obtained from the PARAFAC model

145   were used to calculate the approximate abundance of each component, expressed as F_{max} (in RU),

146   corresponding to the maximum fluorescence intensity for a particular sample.

147   Fluorescence indices based on intensity ratios that provide insight into the origins of dissolved

148   BrC, such as the humification index (HIX) (the ratio of average emission intensity in the 435−480-nm

149   range to that in the 300−345-nm range following excitation at 254 nm, which was used to reflect the

150   degree of humification) (Zsolnay et al., 1999), the biological index (BIX) (the ratio of emission

151   intensities at 380 and 430 nm following excitation at 310 nm, reflecting autochthonous biological

152   activity in water samples) (Huguet et al., 2009), and fluorescence index (FI) (the ratio of emission

153   intensities at 470 and 520 nm following excitation at 370 nm, reflecting the possibility of microbial

154   origin and for examining differences in precursor organic materials) (Lee et al., 2013;Murphy et al.,

155   2018).

156   **2.4. Statistical analysis**

157   A hierarchical cluster method was used to classify aerosol samples based on the relative

158   contributions of PARAFAC components to the respective samples. The Squared Euclidean distance

159   method was used to evaluate the distances between samples, and the Between-group linkage method

160   was chosen for hierarchical cluster analysis. The multiple linear regression (MLR) model was applied

161   to elucidate the relationship between chromophores and light absorption of BrC using a stepwise

162   screening process. Analyses were performed using SPSS software (SPSS Inc., Chicago, IL, USA).

163   **3.   Results and Discussion**

164   **3.1. EEM of dissolved organic substances.**

165   Fluorescence spectra coupled with PARAFAC results can provide more information about the

166   chemical structures of chromophores. Figure 1 and Table S2 show the seven-component (P1–7)

167   PARAFAC solutions of WSOC in the samples of aerosol over Bangkok, the peaks of which fell mainly

168   into the humic-like and protein-like chromophore regions in the plots. Components P2, P3, P4, and P6

169   were identified as humic-like substances (HULIS) (Chen et al., 2017a;Stedmon and Markager,

170   2005;Wu et al., 2019;Chen et al., 2003). A second peak was observed at a high excitation wavelength

171   for these components, indicating the existence of a large number of condensed aromatic moieties,

172   conjugated bonds, and nonlinear ring systems (Matos et al., 2015). Among them, P2, P3, and P4 had a

173   longer emission wavelength (> 400 nm) than P6, likely due to the low probability of fluorescence

174   emission from quinonoid n-π* transitions (Cory and McKnight, 2005). P3 produced similar spectra to

175   those of aqueous reaction products of hydroxyacetone with glycine (Gao and Zhang, 2018), and

176   dissolved organic matter (DOM) in the surface water of Xiangxi Bay and Three Gorges Reservoir

177   (Wang et al., 2019). P6 had a peak similar to those in the fluorescence spectra of N-containing SOA

178   species formed by α-pinene under ozonolysis and photooxidation with NH_3 in a flow reactor (Babar et

179   al., 2017) as well as pyridoxine (Pohlker et al., 2012), indicating a possible biological source. P5 was

180   similar to a previously identified fluorophore in $PM_{2.5}$ from Xi'an (Chen et al., 2019b). P1 and P7

181   could be assigned as protein-like organic matter (PLOM) due to their short emission wavelengths (Wu

182   et al., 2003). Specifically, P7 resembled a tyrosine-like fluorophore (Zhou et al., 2019;Chen et al., 2003)

183   and may be related to non-N-containing species (Chen et al., 2016).

184   The MSOC fraction extracted from the filter residue after water extraction produced fluorescence

185   signals with fluorescence patterns different from those of the WSOC fraction, indicating a different

186   chemical composition from that of WSOC. Thus, WSOC with the addition of MSOC may provide a

187   more comprehensive description of the optical and chemical characteristics of BrC compared to

188   WSOC alone. Six components (C1–C6) were resolved for the MSOC. Among them, C1 and C2 were

189   associated with shorter excitation wavelengths (< 250 nm) but longer emission wavelengths (> 380

190   nm), indicating the presence of fulvic-like substances (Chen et al., 2003;Mounier et al., 1999). C6

191   produced a pattern similar to that of tyrosine-like fluorescence (Stedmon and Markager, 2005).

192   Although C4 had a similar EEM spectrum as P4 of WSOC, the two components were chemically

193   different in polarity, suggesting different behaviors in the environment (Ishii and Boyer, 2012). Note

194   that there were no special chemical structures for the different types of chromophores, and therefore,

195   the origins and chemical structures of HULIS and PLOM studied here are not necessarily like those

196   with the same names in other types of organic matter.
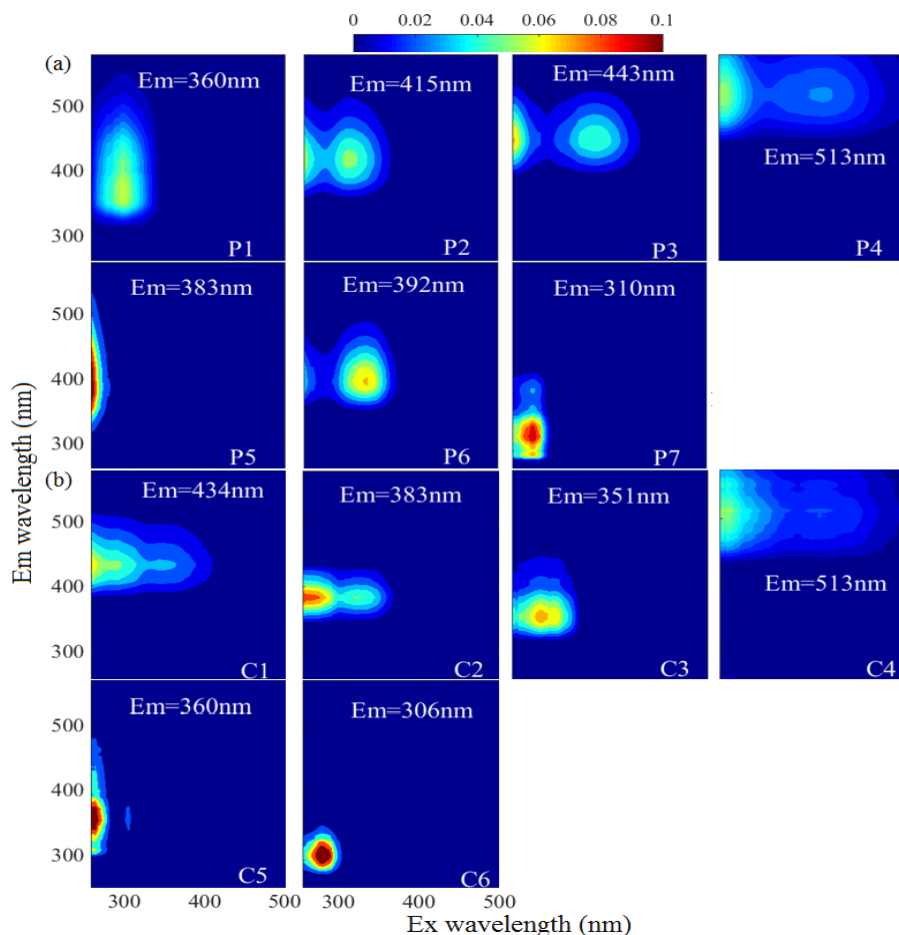
Figure 1. The fluorescent components identified by the PARAFAC (parallel factor) analysis for EEM of water-soluble organic carbon (P1–P7, WSOC, a) and methanol-soluble organic carbon (C1–C6, MSOC, b) in the aerosol samples over Bangkok in Thailand (n=85).

To further explore the potential sources of the EEM-PARAFAC components, we added 60 source samples to the matrices. The source sample EEM data were described in our previous study (Tang et al., 2020b), including those of 33 biomass-burning samples (IDs: 1–33), 17 coal-combustion samples (IDs: 34–50) samples, eight tunnel samples (IDs: 51–58) and two vehicle-exhaust samples from trucks (IDs: 59–60) , which are important sources of BrC in the atmosphere. This, in combination with our Bangkok field samples, yielded a new matrix (145 × 188 × 125, 145-model) for modeling. PARAFAC analysis successfully decomposed the dataset, and the output was the same as for the 85-model. The component solutions are presented in Fig. S6. To validate the stability of the model after loading by the new matrix, the Tucker congruence coefficient (TCC) was calculated to determine the similarity

210   of two fluorescence spectra between the two models (refer to Text S3 of Supplement). Note that a

211   higher TCC value would indicate a higher degree of similarity of the spectra. As shown in Table S2

212   and Fig. S7, high TCC values were found as expected between the 85-model components and the 145-

213   model components, indicating that the two models identified similar chromophores. Although one

214   exceptional component was detected each for the WSOC and MSOC fractions by the new 145-model,

215   these fluorescent components were only highly characterized by source samples, as reported in our

216   previous study (Tang et al., 2020b).

217   Using the distribution proportions of the EEM-PARAFAC fitted components (145-model), we

218   conducted hierarchical cluster analysis of the mixed ambient and source samples. The results are

219   shown in Figs. S9 and S10. For the WSOC fraction, all aerosol samples from Bangkok and tunnel

220   samples were assigned to cluster A, whereas biomass-burning and coal-combustion aerosols were

221   assigned to clusters C and D, respectively. This implied that the chromophore types could be somewhat

222   related to the emission precursors of the aerosol components. However, the distribution of

223   chromophores varied clearly between the ambient aerosols and source samples. The ambient aerosol

224   samples contained higher levels of chromophores with longer emission wavelengths that were related

225   to humic-like or fulvic-like chromophores (components 145M-P1 (P1 component in 145-model),

226   145M-P5, and 145M-P6), whereas the primary biomass-burning and coal-combustion samples

227   contained high-intensity chromophores with shorter emission wavelengths that were related to protein-

228   like fluorescence (145M-P2 and 145M-P4). These phenomena was similarly reported previously, i.e.,

229   protein-like substances produce compounds with similar fluorescence properties as humic substances

230   under irradiation conditions (Bianco et al., 2014). Similar differences between field samples and source

231   samples were found for the MSOC fraction. Therefore, our results confirmed that chemical reactions

232   or "aging" in the atmosphere greatly modifies the chromophore patterns of emission sources by both

233   bleaching the source chromophores or producing new chromophores and, at least in this case, shifts

234   the chromophore emission wavelength toward longer wavelengths, i.e., from protein-like to fulvic-like

235   (Bianco et al., 2014;Bianco et al., 2016;Lee et al., 2013).

236   **3.2. Fluorescence-derived indices**

237   The ratios of fluorescence intensity from specific spectral regions of an EEM were used as

238   indicators for the relative contributions of organic matter derived from terrestrial or microbial sources

239   in natural waters (Shimabuku et al., 2017;Birdwell and Engel, 2010;Mcknight et al., 2001). HIX was

240   initially introduced to estimate the degree of maturation of DOM in soil (Zsolnay et al., 1999),

241   representing the degree of humification of organic matter, for which higher HIX values also indicate

242   higher degree of polycondensation (low H/C ratio) and aromaticity (Qin et al., 2018). Generally, high

Atmospheric
Chemistry
and Physics
Discussions

243 HIX values (> 10) correspond to strongly humified or aromatic organics, principally of terrestrial
244 origin, whereas low values (< 4) are indicative of autochthonous or microbial origin. As shown in
245 Table 1 and Fig. 2, the HIX values were 3.4±0.99 and 2.0±0.59 for WSOC and MSOC, respectively,
246 in aerosol samples from Bangkok. All HIX values were less than 10, which could be viewed as a
247 nominal cutoff below which DOM is not significantly humified (Birdwell and Valsaraj, 2010;Zsolnay
248 et al., 1999;Huguet et al., 2009). Figure 2 shows the HIX values in primary biomass-burning and coal-
249 combustion samples, which were much lower than those in the ambient samples, indicating that the
250 lower values of HIX in the atmosphere likely correspond to freshly introduced material. Lee et al.
251 (2013) reported that fresh SOA had low HIX values, but these values increased significantly upon
252 aging with ammonia. The much higher HIX values in the WSOC compared to the MSOC suggest that
253 WSOC may have a higher degree of aromaticity or a more condensed chemical structure. Our previous
254 study revealed that MSOC has a higher molecular weight but lower aromaticity index than the
255 corresponding WSOC in combustion experiment aerosol samples, indicating a more aliphatic structure
256 in the MSOC (Tang et al., 2020b). The HIX values of WSOC were highest in the hot season (3.9±1.1),
257 followed by the pre-hot season (3.3±1.1), cool season (2.9±0.36), and monsoon (2.5±0.22), whereas
258 those of the MSOC tended to be higher in the hot and cool seasons than in the monsoon and pre-hot
259 seasons. The HIX values in the WSOC fraction were comparable to those of water-soluble organic
260 aerosols in the high Arctic atmosphere (mean: 2.9) (Fu et al., 2015) and higher than those of water-
261 soluble aerosols (1.2±0.1 in winter and 2.0±0.3 in summer) over northwest China (Qin et al., 2018),
262 likely indicating a higher degree of chromophore humification.

263 **Table 1** Seasonal averages of the concentration of organic carbon (OC), elemental carbon (EC), water-soluble organic
264 carbon (WSOC), and methanol-soluble organic carbon (MSOC), BrC absorption, fluorescence indices and
265 levoglucosan level for aerosol samples collected from Bangkok in Thailand. Pre-hot season is from January 18 to
266 February 29, 2016; hot season is from March 2 to May 31, 2016; monsoon is from June 2 to October 30, 2016; cool
267 season is from November 1, 2016 to January 28, 2017.

	Annual (n=85) Ave ± sd	Pre-Hot season (n=7) Ave ± sd	Hot season (n=41) Ave ± sd	Monsoon (n=7) Ave ± sd	Cool season (n=30) Ave ± sd
[a]OC (μg C m^{-3})	12±7.3	19±9.3	9.6±6.7	6.5±0.97	16±5.6
[a]EC (μg C m^{-3})	1.4±0.48	2.0±0.45	1.2±0.47	1.2±0.15	1.5±0.40
[a]OC/EC	8.9±5.2	9.6±3.4	8.4±6.8	5.4±0.51	10±2.5
WSOC					
μg C m^{-3}	6.2±4.2	9.9±5.7	5.3±4.1	2.6±0.31	7.4±3.4
AAE (330–400 nm)	5.1±0.68	5.0±0.52	5.4±0.56	6.2±0.11	4.5±0.34

Abs$_{365}$ (Mm^{-1})	5.6±4.9	10±7.4	4.5±4.5	1.2±0.21	7.2±4.1
MAE$_{365}$ (m^2 g^{-1} C)	0.83±0.25	0.96±0.19	0.78±0.23	0.45±0.06	0.95±0.21
FI	1.6±0.10	1.6±0.09	1.6±0.08	1.7±0.07	1.7±0.07
BIX	0.82±0.13	0.83±0.14	0.74±0.13	0.92±0.05	0.89±0.07
HIX	3.4±0.99	3.3±1.1	3.9±1.1	2.5±0.22	2.9±0.36
			MSOC		
µg C m^{-3}	6.0±3.4	9.2±4.0	4.3±2.9	3.9±0.86	8.1±2.6
AAE (330–400 nm)	5.2±0.94	4.9±0.69	5.5±1.1	5.1±0.15	4.7±0.55
Abs$_{365}$ (Mm^{-1})	1.7±1.4	1.9±1.6	1.0±0.99	0.72±0.23	2.7±1.4
MAE$_{365}$ (m^2 g^{-1} C)	0.26±0.12	0.19±0.08	0.23±0.11	0.19±0.06	0.33±0.11
FI	1.8±0.20	1.5±0.20	1.8±0.23	2.0±0.10	1.8±0.06
BIX	1.2±0.18	1.4±0.20	1.2±0.19	1.3±0.09	1.3±0.14
HIX	2.0±0.59	1.3±0.41	2.1±0.68	1.9±0.17	2.1±0.42
[a]Levoglucosan (ng C m^{-3})	222±485	362±438	185±654	42±16	280±185

268   a: described elsewhere (Wang et al., 2020a).

269
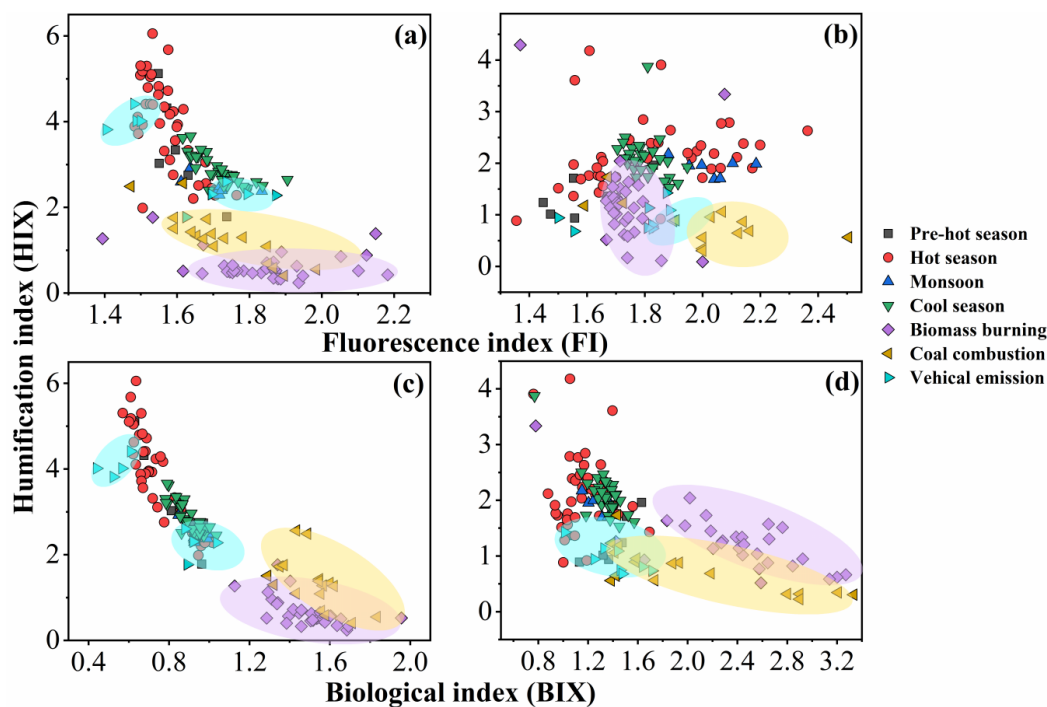
Figure 2. Fluorescence index (FI), biological index (BIX), and humification index (HIX) of water-soluble organic
carbon (WSOC, a, c) and methanol-soluble organic carbon (MSOC, b, d) in aerosol samples from Bangkok, Thailand,

Atmospheric
Chemistry
and Physics
Discussions

272   as well as source emission samples including biomass burning, coal combustion and vehicle emission which were

273   encircled by a violet, yellow, and blue region, respectively. Note that the fluorescence characteristic of source samples

274   was described elsewhere (Tang et al., 2020b), but the fluorescence indices was first reported in this study. Pre-hot

275   season is from January 18 to February 29, 2016; hot season is from March 2 to May 31, 2016; monsoon is from June

276   2 to October 30, 2016; cool season is from November 1, 2016 to January 28, 2017.

277   The BIX and FI were previously proposed as proxies for the contribution of biogenic organic

278   matter and autochthonous biological activity in natural water, respectively (Fu et al., 2015;Qin et al.,

279   2018). For example, the FI decreased by up to 20% indicating that the samples appeared increasingly

280   like "terrestrial" DOM, whereas the BIX increased by up to 37% indicating that the samples became

281   more "autochthonous" in character (Murphy et al., 2018;Gabor et al., 2014). FI values ≤ 1.4 correspond

282   to terrestrially derived organics and higher aromaticity, whereas values ≥ 1.9 correspond to microbial

283   sources and a lower aromatic carbon content (Mcknight et al., 2001). An increase in BIX is related to

284   an increase in the contribution of microbially derived organics, with high values (> 1) shown to

285   correspond to a predominantly biological or microbial origin of DOM and the presence of organic

286   matter freshly released into water, whereas values ≤ 0.6 indicate the presence of little biological

287   material (Huguet et al., 2009).

288   The FI and BIX values of the Bangkok aerosol samples are summarized in Table 1 and Fig. 2.

289   The FI values of the WSOC and MSOC were 1.6±0.10 and 1.8±0.20, respectively, suggesting that

290   these chromophores are representative of both terrestrially and microbially derived organic matter. The

291   BIX values of the WSOC and MSOC were 0.82±0.13 and 1.2±0.18, respectively. Almost all BIX

292   values were greater than 0.6 in the two fractions, suggesting biological or microbial contribution. Lee

293   et al. (2013) reported that the BIX values of SOA samples averaged 0.6 and increased upon aging. In

294   addition, the results of our source samples showed that primary biomass-burning and coal-combustion

295   samples had high FI and BIX values (Fig. 2). These results indicate that these chromophores in

296   Bangkok were likely freshly introduced or derived from biomass burning and coal combustion. Further,

297   an increase in BIX in the MSOC in comparison with the WSOC was observed in primary biomass-

298   burning and coal-combustion samples, consistent with the Bangkok samples. The BIX values were

299   similar to those in the WSOC in Arctic aerosols (0.6–0.96, mean: 0.72), which were within the extreme

300   values for the predominance of humic- or protein-like fluorophores (Fu et al., 2015). BIX values

301   exhibited the opposite trend from HIX values, with low BIX values in the hot season. This may be

302   explained by a previous study showing that a high BIX appears to indicate little humification (Birdwell

303   and Engel, 2010). It should be noted that the fluorescence indices (FI, BIX, and HIX) were first applied

304   for aquatic and soil organic compounds and further extended to the atmosphere due to the similarities

305   in the properties of organic matter (Graber and Rudich, 2006). However, the values observed for

306 primary biomass burning and coal combustion in this study differ from with the previously established

307 fluorescence standards for aquatic environments and soil. Therefore, caution is required when using

308 these indices to appoint source of atmospheric chromophores (Wu et al., 2021).

309 **3.3. Optical properties of dissolved BrC.**

310 Figure 3 shows the variations in soluble OC concentrations and the corresponding light absorption

311 coefficient at 365 nm (Abs_{365}). In general, the Abs_{365} closely tracked the variations in the mass

312 concentrations of WSOC and MSOC ($p < 0.000$, $R^2 = 0.95$ and $p < 0.000$, $R^2 = 0.75$, respectively) (Fig.

313 S11), indicating that the portions of BrC in both fractions were considerably stable.

314
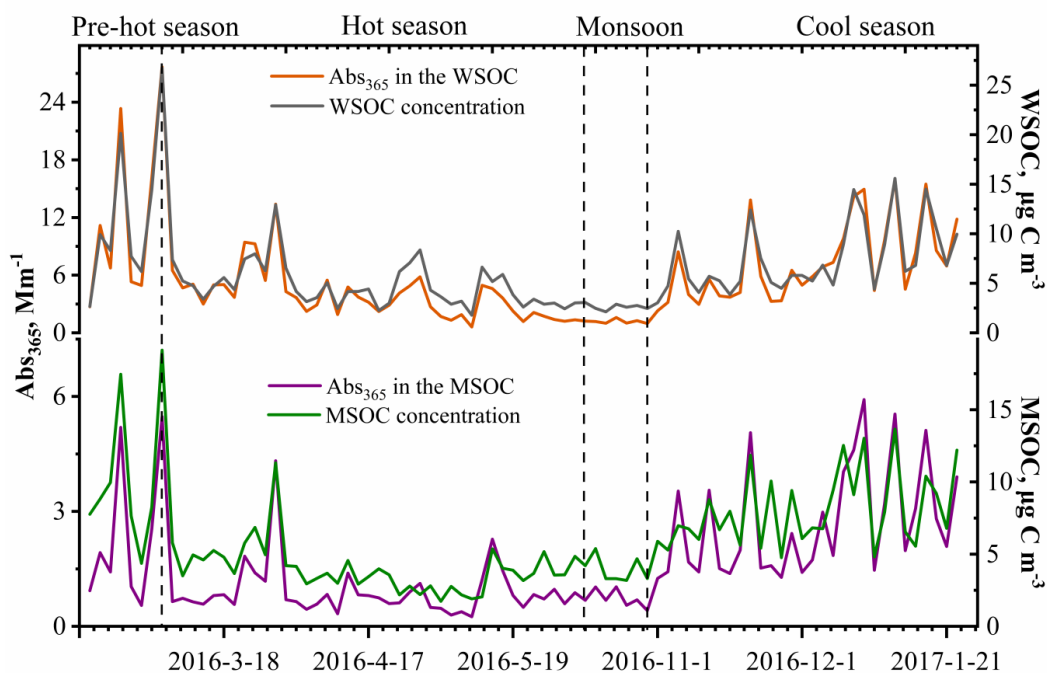
Figure 3. Time series plots of water-soluble organic carbon (WSOC) and methanol-soluble organic carbon (MSOC)

concentration ($\mu g\ C\ m^{-3}$) and water- and methanol-extract light absorption coefficient at 365 nm (Abs_{365}) (Mm^{-1}) in

the aerosol samples from Bangkok, Thailand during 2016–2017.

318 The absorption Ångström exponent (AAE) and mass absorption efficiency (MAE) are important

319 optical parameters reflecting the spectral dependence and light absorption ability of BrC, respectively.

320 The magnitude of the AAE reflects the differences in BrC source and atmospheric processes (Lack et

321 al., 2013). Typically, the AAE value is close to 1 when light absorption is dominated by soot

322 (Kirchstetter et al., 2004), roughly 1–3 for simulated biomass-burning aerosols (Hopkins et al., 2007),

323 and up to 6–7 for water-soluble HULIS in biomass burning-impacted aerosols (Hoffer et al., 2006).

324 The AAE values of the WSOC and MSOC between 330 and 400 nm in this study were up to 5.1±0.68

325 and 5.2±0.94 (Fig. 4), respectively, indicating strong wavelength dependence in the light absorption

326 capability. These high values show that BrC tends to absorb more solar irradiation over ultraviolet

327 wavelengths, which is comparable to BC absorption as shown in Fig. S12. These observations indicate

328 that BrC has important impacts on photochemical reactions in the atmosphere (Barnard et al., 2008).

329 The AAE values in this study are similar to those of water-soluble BrC over biomass burning-impacted

330 regions, such as Beijing (Mo et al., 2018;Yan et al., 2015) and Guangzhou (Liu et al., 2018), but lower

331 than those of aerosols from simulated biomass-burning and coal-combustion experiments (Fan et al.,

332 2018;Tang et al., 2020a;Li et al., 2018). However, it should be noted that the BrC AAE varies in the

333 atmosphere. Dasari et al. (2019) reported that AAE values of water-soluble BrC increase continuously

334 due to photolysis of chromophores and atmospheric oxidation during long-range transport over the

335 Indo-Gangetic Plain (IGP). In addition, pH changes can cause the absorption spectra of some BrC

336 species to shift to longer wavelengths upon deprotonation, decreasing AAE values (Mo et al., 2017).
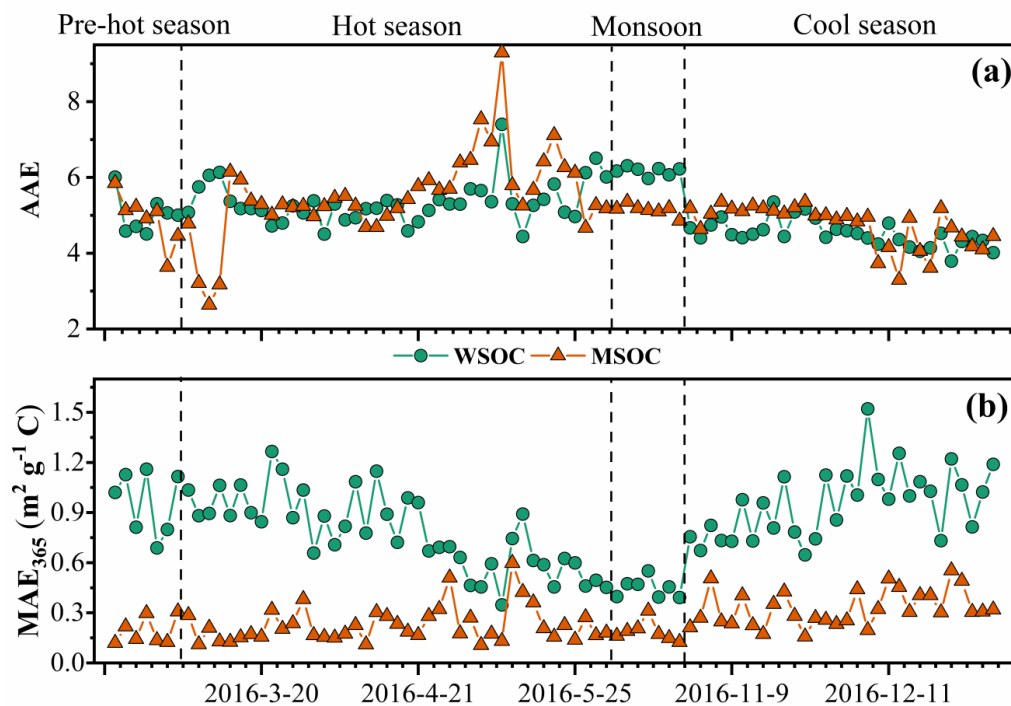
337

338 **Figure 4.** Time series plots of Absorption Ångström exponent (AAE, a), the mass absorption efficiency at 365 nm

339 (MAE_{365}, b) in the water-soluble organic carbon (WSOC) and methanol-soluble organic carbon (MSOC) in aerosols

340 samples from Bangkok in Thailand during 2016–2017.

Atmospheric
Chemistry
and Physics
Discussions

341   The MAE at 365 nm (MAE_{365}) of the WSOC was 0.83±0.25 m^2 g^{-1} C, which was higher than that

342   of the MSOC (0.26±0.12 m^2 g^{-1} C), indicating that more water-soluble BrC with stronger light

343   absorption capability could be extracted with ultrapure deionized water, whereas water-insoluble BrC

344   is characterized by lower light absorption capability over Bangkok. These results were consistent with

345   those from vehicular exhaust samples in our previous study, where MAE_{365} values of the WSOC

346   (0.71±0.30 m^2 g^{-1} C) were higher than those of the MSOC (0.26±0.09 m^2 g^{-1} C) (Tang et al., 2020b).

347   Opposite results have been shown for primary biomass burning and coal combustion (Tang et al.,

348   2020b). Wu et al. (2020b) reported that the MAE values of MSOC are higher than those of WSOC in

349   summer, whereas the situation is reversed in winter. As not all water-insoluble components can be

350   extracted with methanol, the observed light absorption by MSOC would therefore likely reflect the

351   lower limit. Table S3 shows a comparison of the MAE values of Bangkok aerosols with those of other

352   regions, indicating a medium light absorption capacity. The MAE_{365} values of the water-soluble

353   fraction in this study were comparable to those of Nanjing (Chen et al., 2018), Guangzhou (Liu et al.,

354   2018), and Beijing in summer (Yan et al., 2015), but lower than those of $PM_{2.5}$ from Singapore (Adam

355   et al., 2020), PM_{10} from Godavari, Nepal, in the pre-monsoon season (Wu et al., 2019), and smoke

356   particles from biomass burning and coal combustion (Park and Yu, 2016;Fan et al., 2018;Tang et al.,

357   2020b). Lower MAE_{365} values of both fractions were observed in the monsoon season than in the non-

358   monsoon seasons, likely due to the heavy monsoon rains that effectively remove soluble gases and

359   aerosols (Lawrence and Lelieveld, 2010) and/or reduce biomass-burning activity (levoglucosan level

360   in Table 1). A previous study reported similar findings in the USA in that the MAE_{365} was

361   approximately three-fold higher in biomass burning-impacted samples than in non-biomass burning-

362   impacted samples (Hecobian et al., 2010). Another study in the central Tibetan Plateau highlighted that

363   BrC emitted by biomass burning has stronger light absorption capability than does secondary BrC

364   formed in the atmosphere (Wu et al., 2018). On the Indo-China peninsula, Bangkok receives 99% of

365   the fire-derived aerosols from December to April (Lee et al., 2017), which may explain the high

366   absorption levels in the non-monsoon seasons.

367   **3.4. Chromophores responsible for BrC light absorption.**

368   EEM analysis enables the probing of the chemical structure of DOM because of its ability to

369   distinguish among different classes of organic matter (Wu et al., 2003). Generally, BrC absorption is

370   related to the chromophores within it and is susceptible to change with variations in chemical

371   properties, e.g., oxidation level (Mo et al., 2018), degree of unsaturation (Jiang et al., 2020), molecular

372   weight (Tang et al., 2020b;Di Lorenzo et al., 2017), functional groups (Chen et al., 2017b), molecular

373   composition, etc (Song et al., 2019;Lin et al., 2018). The fluorescence intensity of each EEM

374   component was shown to be associated with light absorption indices, such as MAE_{365} and AAE, of

375   HULIS in controlled crop straw-combustion experiments (Huo et al., 2018). As a linear relationship

376   between organic matter concentration and fluorescence intensity can be assumed for very dilute

377   samples due to the IFE (Murphy et al., 2013), we have corrected our fluorescence data for IFE using

378   absorbance to enable "clean " correlation analysis (as shown in Fig. S13 a, b). The linear regression

379   slopes in the scatter plots of Abs_{365} versus WSOC or MSOC could mathematically represent the

380   average MAE values of WSOC or MSOC at 365 nm, respectively (Fig. S11 a, b). The phenomenon

381   indicates that both fluorescence and Abs_{365} data point to similar relationships between sources or

382   chemical processes with organic matter concentrations, and therefore, we attempted to link the

383   fluorescence results to BrC absorption. It should be noted that light-absorbing substances in

384   atmospheric particulate matter are not necessarily all fluorescent, such as nitrophenol compounds,

385   which are a type of BrC commonly found in the atmospheric particulate matter; however, there is no

386   strong fluorescence signal with which to scan the nitrophenol standards (Chen et al., 2019a).

387   We used MLR to explore the relationship between the fluorescence intensities of chromophores

388   and Abs_{365}. During MLR, insignificant fluorescent components were excluded from the regression

389   using a stepwise screening process to avoid overfitting ($F_{inclusion}$: $p < 0.05$; $F_{elimination}$: $p > 0.10$). The

390   MLR statistical metrics are listed in Tables S4 and S5. For the WSOC fraction, a revised model

391   (regression 3) equation was used with an adjusted R^2 of 0.995. The final optimized equations were

392    $Abs_{365} = 0.765 \times P4 + 0.051 \times P2 + 0.091 \times P7$, for the WSOC fraction, and $Abs_{365} = 0.238 \times C4$ for

393   the MSOC fraction (Table S5). The model errors for water-soluble and methanol-soluble Abs_{365} were

394   −5.5%–64% and −34%–58%, respectively. The predicted Abs_{365} values fit the measured values well

395   (Fig. 5, slope = 0.99 and 0.95, and R^2 = 0.99 and 0.94 for WSOC and MSOC, respectively).
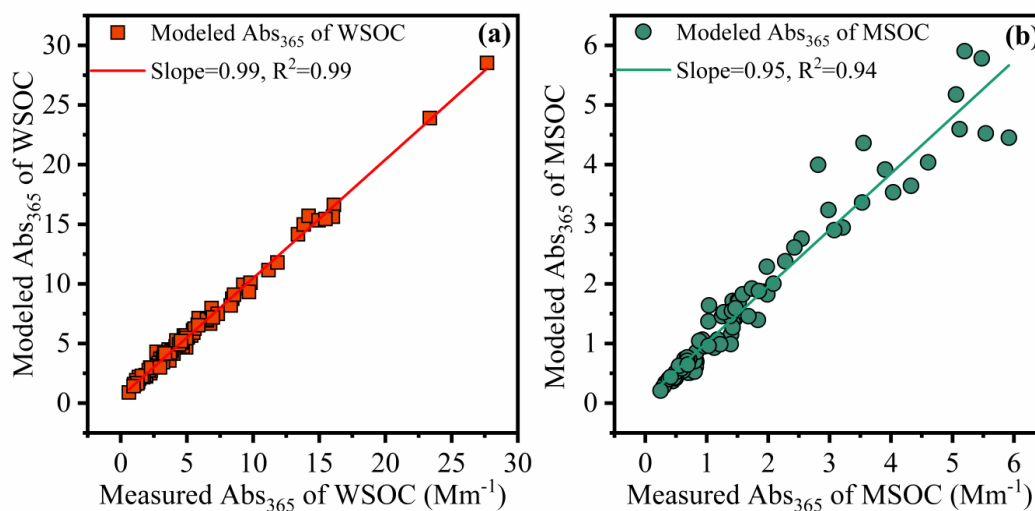
Figure 5. Linear correlation analysis between modeling Abs_{365} using multiple linear regression (MLR) analysis and measured Abs_{365} in the water-soluble organic carbon (WSOC, a) and methanol-soluble organic carbon (MSOC, b) in aerosols samples from Bangkok in Thailand during 2016–2017, respectively. Note that the fluorescent intensities of parallel factor (PARAFAC) model results (fluorescent components) were used as variables in MLR analysis.

For water-soluble BrC, the P4 component had the largest coefficient with Abs_{365}, which was much higher than those for P2 and P7. The C4 component had the largest coefficient with Abs_{365} for methanol-soluble BrC. These results indicate that the light absorption by BrC is more dependent on chromophores with longer emission wavelengths (P4 and C4). These characteristics also indicate that the strongly absorbing substances in BrC probably originate from large conjugated electron functional groups or include donor and acceptor molecules for charge-transfer interactions (Del Vecchio and Blough, 2004;Cory and McKnight, 2005). Kellerman et al. (2015) reported that these components are highly aromatic and oxygen-rich with high apparent molecular weight. These important findings highlight that larger chromophores may be the most persistent BrC species in the atmosphere and hence exert the greatest influence for perturbing the global radiative balance.

To further interpret the BrC source profiles as real-world TSP sources, we examined 84 (minus one missing value) TSP samples from Bangkok using the US EPA PMF5.0 model. All samples were merged together to form an 84 × 30 dataset (84 samples with 30 species). The initial data of positive matrix factorization input were from our previous study (Wang et al., 2020a). We further added Abs_{365} values of WSOC and MSOC, and the fluorescence intensities (in RU) of P2, P4, P7, and C4 components to the model. A seven-factor solution was achieved that provided the most physically reasonable source profiles (Fig. S14), including ship emission, secondary sulfate, dust, land fossil-fuel combustion, sea salt, biomass burning, and industrial emission, consistent with our previous study

419   (Wang et al., 2020a). Figure S14 also shows the contributions of the above sources to light absorption

420   at λ= 365 nm, which represent the fraction of BrC for each factor. Biomass burning was found to be

421   the main source of BrC over Bangkok; 61% and 67% for water-soluble and methanol-soluble BrC,

422   respectively. These were comparable to previous observations using a similar approach in Xi'an (55%)

423   (Wu et al., 2020a). Furthermore, the P4 and C4 components, which were more closely associated with

424   Abs$_{365}$, could be mostly attributed to biomass burning (64% and 66%, respectively) as shown in Fig.

425   6. Our previous study showed that biomass burning accounted for a considerably large portion (mean:

426   26%) of the TSP mass concentration in the same samples (Wang et al., 2020a). This result suggests

427   that biomass burning makes a significant contribution to not only particulate matter but also BrC light

428   absorption.

429
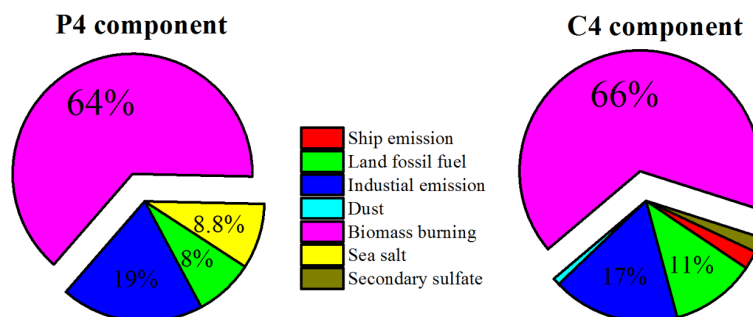
Figure 6. Positive matrix factorization derived source apportionment of chromophores P4 of the WSOC and C4 of
431   the MSOC in TSP samples over Bangkok in Thailand during 2016–2017.

432   **4. Conclusions**

433   This study presents a comprehensive analysis of water- and methanol-soluble chromophores in

434   aerosol samples over Bangkok in Thailand during 2016–2017. EEM combining with PARAFAC

435   analysis showed that the identified fluorescent components were humic-like and protein-like

436   substances but different patterns in the WSOC and MSOC, indicating different chemical compositions.

437   By adding three-source fluorescence into the original PARAFAC model, we found that chromophores

438   with longer emission wavelengths in the atmosphere may be due to atmospheric chemical reactions or

439   "aging" by both bleaching the source chromophores or producing new chromophores. We also suggest

440   that caution is required when using fluorescence indices to appoint source of atmospheric

441   chromophores. In addition, more water-soluble BrC with stronger light absorption capability could be

442   extracted with ultrapure deionized water over Bangkok (0.83±0.25 vs. 0.26±0.12 m^2 g^{-1} C), and both

443   water-soluble and methanol-soluble BrC exhibited a high light-absorption in non-monsoon seasons

444   due to the influence of biomass burning. The MLR analysis showed that both the light absorption of

445 BrC at 365 nm in the two fractions was significantly dependent on the special chromophores with
446 longer emission wavelength that are generally highly aromatic and oxygen-rich with high apparent
447 molecular weight. Positive matrix factorization model results further showed that biomass burning was
448 main contributor of these chromophores (up to 60%). In summary, this study provides a new insight
449 into BrC absorption and sources, which may promote the application of EEM spectroscopy to predict
450 and model the light absorption of BrC in the atmosphere.

451 *Data availability.* The data used in this study are available upon request. Please contact Guangcai
452 Zhong (gczhong@gig.ac.cn).

453 *Supplement.* The supplement related to this article is available.

454 *Author contributions.* JT, GZ, JL, and GZ (Guangcai Zhong) designed the experiment. JT and JW
455 carried out the measurements and analyzed the data. JW and SB organized and performed the
456 samplings. JT (Jianhui Tang) supported the fluorescence instruments and laboratory. CT and HJ
457 supported the models. JT wrote the paper. JL, GZ (Guangcai Zhong), YC, YM, BZ, XG, and GZ
458 reviewed and commented on the paper.

459 *Competing interests.* The authors declare that they have no conflict of interest.

465 **References**

466 Adam, M. G., Chiang, A. W. J., and Balasubramanian, R.: Insights into characteristics of light absorbing
467 carbonaceous aerosols over an urban location in Southeast Asia, Environ. Pollut., 257, 113425,
468 https://doi.org/10.1016/j.envpol.2019.113425, 2020.
469 Alexander, D. T. L., Crozier, P. A., and Anderson, J. R.: Brown carbon spheres in East Asian outflow and their optical
470 properties, Science, 321, 833-836, https://10.1126/science.1155296, 2008.
471 Andersson, C. A., and Bro, R.: The N-way Toolbox for MATLAB, Chemom. Intell. Lab. Syst., 52, 1-4,
472 https://doi.org/10.1016/s0169-7439(00)00071-x, 2000.
473 Babar, Z. B., Park, J.-H., and Lim, H.-J.: Influence of NH 3 on secondary organic aerosols from the ozonolysis and
474 photooxidation of α-pinene in a flow reactor, Atmos. Environ., 164, 71-84,
475 https://10.1016/j.atmosenv.2017.05.034, 2017.
476 Bahram, M., Bro, R., Stedmon, C., and Afkhami, A.: Handling of Rayleigh and Raman scatter for PARAFAC
477 modeling of fluorescence data using interpolation, J. Chemom., 20, 99-105, https://doi.org/10.1002/cem.978,

Atmospheric
Chemistry
and Physics
Discussions

478   2006.

479   Barnard, J. C., Volkamer, R., and Kassianov, E. I.: Estimation of the mass absorption cross section of the organic
480   carbon component of aerosols in the Mexico City Metropolitan Area, Atmos. Chem. Phys., 8, 6665-6679,
481   http://10.5194/acp-8-6665-2008, 2008.

482   Bianco, A., Minella, M., De Laurentiis, E., Maurino, V., Minero, C., and Vione, D.: Photochemical generation of
483   photoactive compounds with fulvic-like and humic-like fluorescence in aqueous solution, Chemosphere, 111,
484   529-536, https://10.1016/j.chemosphere.2014.04.035, 2014.

485   Bianco, A., Passananti, M., Deguillaume, L., Mailhot, G., and Brigante, M.: Tryptophan and tryptophan-like
486   substances in cloud water: Occurrence and photochemical fate, Atmos. Environ., 137, 53-61,
487   https://10.1016/j.atmosenv.2016.04.034, 2016.

488   Birdwell, J. E., and Engel, A. S.: Characterization of dissolved organic matter in cave and spring waters using UV–
489   Vis absorbance and fluorescence spectroscopy, Org. Geochem., 41, 270-280,
490   https://10.1016/j.orggeochem.2009.11.002, 2010.

491   Birdwell, J. E., and Valsaraj, K. T.: Characterization of dissolved organic matter in fogwater by excitation–emission
492   matrix fluorescence spectroscopy, Atmos. Environ., 44, 3246-3253, https://10.1016/j.atmosenv.2010.05.055,
493   2010.

494   Chen, H., Liao, Z. L., Gu, X. Y., Xie, J. Q., Li, H. Z., and Zhang, J.: Anthropogenic Influences of Paved Runoff and
495   Sanitary Sewage on the Dissolved Organic Matter Quality of Wet Weather Overflows: An Excitation-Emission
496   Matrix Parallel Factor Analysis Assessment, Environ. Sci. Technol., 51, 1157-1167,
497   https://doi.org/10.1021/acs.est.6b03727, 2017a.

498   Chen, Q., Miyazaki, Y., Kawamura, K., Matsumoto, K., Coburn, S., Volkamer, R., Iwamoto, Y., Kagami, S., Deng,
499   Y., Ogawa, S., Ramasamy, S., Kato, S., Ida, A., Kajii, Y., and Mochida, M.: Characterization of Chromophoric
500   Water-Soluble Organic Matter in Urban, Forest, and Marine Aerosols by HR-ToF-AMS Analysis and Excitation-
501   Emission Matrix Spectroscopy, Environ. Sci. Technol., 50, 10351-10360,
502   https://doi.org/10.1021/acs.est.6b01643, 2016.

503   Chen, Q., Ikemori, F., Nakamura, Y., Vodicka, P., Kawamura, K., and Mochida, M.: Structural and Light-Absorption
504   Characteristics of Complex Water-Insoluble Organic Mixtures in Urban Submicrometer Aerosols, Environ. Sci.
505   Technol., 51, 8293-8303, https://doi.org/10.1021/acs.est.7b01630., 2017b.

506   Chen, Q., Mu, Z., Song, W., Wang, Y., Yang, Z., Zhang, L., and Zhang, Y. L.: Size‐Resolved Characterization of
507   the Chromophores in Atmospheric Particulate Matter From a Typical Coal–Burning City in China, J. Geophys.
508   Res.-Atmos., 124, 10546-10563, https://10.1029/2019jd031149, 2019a.

509   Chen, Q., Wang, M., Wang, Y., Zhang, L., Li, Y., and Han, Y.: Oxidative Potential of Water-Soluble Matter Associated
510   with Chromophoric Substances in PM2.5 over Xi'an, China, Environ. Sci. Technol., 53, 8574-8584,
511   https://10.1021/acs.est.9b01976, 2019b.

512   Chen, W., Westerhoff, P., Leenheer, J. A., and Booksh, K.: Fluorescence excitation - Emission matrix regional
513   integration to quantify spectra for dissolved organic matter, Environ. Sci. Technol., 37, 5701-5710,
514   https://10.1021/es034354c 2003.

515   Chen, Y., and Bond, T. C.: Light absorption by organic carbon from wood combustion, Atmos. Chem. Phys., 10,

516   1773-1787, https://10.5194/acp-10-1773-2010, 2010.

517   Chen, Y., Ge, X., Chen, H., Xie, X., Chen, Y., Wang, J., Ye, Z., Bao, M., Zhang, Y., and Chen, M.: Seasonal light
518   absorption properties of water-soluble brown carbon in atmospheric fine particles in Nanjing, China, Atmos.
519   Environ., 230-240, https://doi.org/10.1016/j.atmosenv.2018.06.002, 2018.

520   Cory, R. M., and McKnight, D. M.: Fluorescence spectroscopy reveals ubiquitous presence of oxidized and reduced
521   quinones in dissolved organic matter, Environ. Sci. Technol., 39, 8142-8149, https://10.1021/es0506962, 2005.

522   Dasari, S., Andersson, A., Bikkina, S., Holmstrand, H., Budhavant, K., Satheesh, S., Asmi, E., Kesti, J., Backman, J.,
523   Salam, A., Bisht, D. S., Tiwari, S., Hameed, Z., and Gustafsson, O.: Photochemical degradation affects the light
524   absorption of water-soluble brown carbon in the South Asian outflow, Sci. Adv., 5, 10,
525   https://10.1126/sciadv.aau8066, 2019.

526   Del Vecchio, R., and Blough, N. V.: On the Origin of the Optical Properties of Humic Substances, Environ. Sci.
527   Technol., 38, 3885-3891, https://10.1021/es049912h, 2004.

528   Di Lorenzo, R. A., Washenfelder, R. A., Attwood, A. R., Guo, H., Xu, L., Ng, N. L., Weber, R. J., Baumann, K.,
529   Edgerton, E., and Young, C. J.: Molecular-Size-Separated Brown Carbon Absorption for Biomass-Burning
530   Aerosol at Multiple Field Sites, Environ. Sci. Technol., 51, 3128-3137, https://10.1021/acs.est.6b06160, 2017.

531   Fan, X., Li, M., Cao, T., Cheng, C., Li, F., Xie, Y., Wei, S., Song, J., and Peng, P. a.: Optical properties and oxidative
532   potential of water- and alkaline-soluble brown carbon in smoke particles emitted from laboratory simulated
533   biomass burning, Atmos. Environ., 194, 48-57, https://10.1016/j.atmosenv.2018.09.025, 2018.

534   Fan, X. J., Cao, T., Yu, X. F., Wang, Y., Xiao, X., Li, F. Y., Xie, Y., Ji, W. C., Song, J. Z., and Peng, P. A.: The
535   evolutionary behavior of chromophoric brown carbon during ozone aging of fine particles from biomass burning,
536   Atmos. Chem. Phys., 20, 4593-4605, https://10.5194/acp-20-4593-2020, 2020.

537   Fu, P., Kawamura, K., Chen, J., Qin, M., Ren, L., Sun, Y., Wang, Z., Barrie, L. A., Tachibana, E., Ding, A., and
538   Yamashita, Y.: Fluorescent water-soluble organic aerosols in the High Arctic atmosphere, Sci Rep, 5, 9845,
539   https://doi.org/10.1038/srep09845, 2015.

540   Fujii, Y., Iriana, W., Oda, M., Puriwigati, A., Tohno, S., Lestari, P., Mizohata, A., and Huboyo, H. S.: Characteristics
541   of carbonaceous aerosols emitted from peatland fire in Riau, Sumatra, Indonesia, Atmos. Environ., 87, 164-169,
542   https://doi.org/10.1016/j.atmosenv.2014.01.037, 2014.

543   Gabor, R. S., Baker, A., McKnight, D. M., and Miller, M. P.: Fluorescence Indices and Their Interpretation, in:
544   Aquatic Organic Matter Fluorescence, edited by: Baker, A., Reynolds, D. M., Lead, J., Coble, P. G., and Spencer,
545   R. G. M., Cambridge Environmental Chemistry Series, Cambridge University Press, Cambridge, 303-338, 2014.

546   Gao, Y., and Zhang, Y.: Formation and photochemical investigation of brown carbon by hydroxyacetone reactions
547   with glycine and ammonium sulfate, RSC Advances, 8, 20719-20725, https://10.1039/c8ra02019a, 2018.

548   Graber, E. R., and Rudich, Y.: Atmospheric HULIS: How humic-like are they? A comprehensive and critical review,
549   Atmos. Chem. Phys., 6, 729-753, https://10.5194/acp-6-729-2006, 2006.

550   Gu, Q., and Kenny, J. E.: Improvement of Inner Filter Effect Correction Based on Determination of Effective
551   Geometric Parameters Using a Conventional Fluorimeter, Anal. Chem., 81, 420-426,
552   https://doi.org/10.1021/ac801676j, 2009.

553   Han, H., Kim, G., Seo, H., Shin, K.-H., and Lee, D.-H.: Significant seasonal changes in optical properties of brown

554   carbon in the midlatitude atmosphere, Atmos. Chem. Phys., 20, 2709-2718, https://10.5194/acp-20-2709-2020,
555   2020.

556 Hawkes, J. A., Patriarca, C., Sjöberg, P. J. R., Tranvik, L. J., and Bergquist, J.: Extreme isomeric complexity of
557   dissolved organic matter found across aquatic environments, Limnol. Oceanogr. Lett., 3, 21-30,
558   https://10.1002/lol2.10064, 2018.

559 Hecobian, A., Zhang, X., Zheng, M., Frank, N., Edgerton, E. S., and Weber, R. J.: Water-Soluble Organic Aerosol
560   material and the light-absorption characteristics of aqueous extracts measured over the Southeastern United
561   States, Atmos. Chem. Phys., 10, 5965-5977, https://10.5194/acp-10-5965-2010, 2010.

562 Hoffer, A., Gelencsér, A., Guyon, P., Kiss, G., Schmid, O., Frank, G., Artaxo, P., and Andreae, M.: Optical properties
563   of humic-like substances (HULIS) in biomass-burning aerosols, Atmos. Chem. Phys., 6, 3563-3570,
564   https://10.5194/acp-6-3563-2006, 2006.

565 Hopkins, R. J., Lewis, K., Desyaterik, Y., Wang, Z., Tivanski, A. V., Arnott, W. P., Laskin, A., and Gilles, M. K.:
566   Correlations between optical, chemical and physical properties of biomass burn aerosols, Geophys. Res. Lett.,
567   34, https://10.1029/2007gl030502, 2007.

568 Huang, K., Fu, J. S., Hsu, N. C., Gao, Y., Dong, X., Tsay, S.-C., and Lam, Y. F.: Impact assessment of biomass burning
569   on air quality in Southeast and East Asia during BASE-ASIA, Atmos. Environ., 78, 291-302,
570   https://doi.org/10.1016/j.atmosenv.2012.03.048, 2013.

571 Huguet, A., Vacher, L., Relexans, S., Saubusse, S., Froidefond, J. M., and Parlanti, E.: Properties of fluorescent
572   dissolved organic matter in the Gironde Estuary, Org. Geochem., 40, 706-719,
573   https://10.1016/j.orggeochem.2009.03.002, 2009.

574 Huo, Y., Li, M., Jiang, M., and Qi, W.: Light absorption properties of HULIS in primary particulate matter produced
575   by crop straw combustion under different moisture contents and stacking modes, Atmos. Environ., 191, 490-
576   499, https://10.1016/j.atmosenv.2018.08.038, 2018.

577 Ishii, S. K., and Boyer, T. H.: Behavior of reoccurring PARAFAC components in fluorescent dissolved organic matter
578   in natural and engineered systems: a critical review, Environ. Sci. Technol., 46, 2006-2017,
579   https://10.1021/es2043504, 2012.

580 Jiang, H., Li, J., Chen, D., Tang, J., Cheng, Z., Mo, Y., Su, T., Tian, C., Jiang, B., Liao, Y., and Zhang, G.: Biomass
581   burning organic aerosols significantly influence the light absorption properties of polarity-dependent organic
582   compounds in the Pearl River Delta Region, China, Environ. Int., 144, 106079,
583   https://doi.org/10.1016/j.envint.2020.106079, 2020.

584 Kasthuriarachchi, N. Y., Rivellini, L.-H., Chen, X., Li, Y. J., and Lee, A. K. Y.: Effect of relative humidity on
585   secondary brown carbon formation in aqueous droplets, Environ. Sci. Technol., 54, 13207-13216,
586   https://10.1021/acs.est.0c01239, 2020.

587 Kellerman, A. M., Kothawala, D. N., Dittmar, T., and Tranvik, L. J.: Persistence of dissolved organic matter in lakes
588   related to its molecular characteristics, Nat. Geosci., 8, 454-U452, https://10.1038/ngeo2440, 2015.

589 Kirchstetter, T. W., Novakov, T., and Hobbs, P. V.: Evidence that the spectral dependence of light absorption by
590   aerosols is affected by organic carbon, J. Geophys. Res.-Atmos., 109, https://10.1029/2004jd004999, 2004.

591 Kirchstetter, T. W., and Thatcher, T. L.: Contribution of organic carbon to wood smoke particulate matter absorption

592   of solar radiation, Atmos. Chem. Phys., 12, 5803-5816, https://doi.org/10.5194/acp-12-6067-2012, 2012.

593 Lack, D. A., Bahreini, R., Langridge, J. M., Gilman, J. B., and Middlebrook, A. M.: Brown carbon absorption linked
594   to organic mass tracers in biomass burning particles, Atmos. Chem. Phys., 13, 2415-2422, https://10.5194/acp-
595   13-2415-2013, 2013.

596 Laskin, A., Laskin, J., and Nizkorodov, S. A.: Chemistry of atmospheric brown carbon, Chem. Rev., 115, 4335-4382,
597   https://doi.org/10.1021/cr5006167, 2015.

598 Laskin, J., Laskin, A., and Nizkorodov, S. A.: Mass Spectrometry Analysis in Atmospheric Chemistry, Anal. Chem.,
599   90, 166-189, https://10.1021/acs.analchem.7b04249, 2018.

600 Lawrence, M. G., and Lelieveld, J.: Atmospheric pollutant outflow from southern Asia: a review, Atmos. Chem. Phys.,
601   10, 11017-11096, https://10.5194/acp-10-11017-2010, 2010.

602 Lee, H.-H., Bar-Or, R. Z., and Wang, C.: Biomass burning aerosols and the low-visibility events in Southeast Asia,
603   Atmos. Chem. Phys., 17, 965-980, https://10.5194/acp-17-965-2017, 2017.

604 Lee, H. J., Laskin, A., Laskin, J., and Nizkorodov, S. A.: Excitation-emission spectra and fluorescence quantum yields
605   for fresh and aged biogenic secondary organic aerosols, Environ. Sci. Technol., 47, 5763-5770,
606   https://10.1021/es400644c, 2013.

607 Li, M., Fan, X., Zhu, M., Zou, C., Song, J., Wei, S., Jia, W., and Peng, P.: Abundances and light absorption properties
608   of brown carbon emitted from residential coal combustion in China, Environ. Sci. Technol., 53, 595-603,
609   https://doi.org/10.1021/acs.est.8b05630, 2018.

610 Lin, P., Laskin, J., Nizkorodov, S. A., and Laskin, A.: Revealing Brown Carbon Chromophores Produced in Reactions
611   of Methylglyoxal with Ammonium Sulfate, Environ. Sci. Technol., 49, 14257-14266,
612   https://doi.org/10.1021/acs.est.5b03608, 2015.

613 Lin, P., Aiona, P. K., Li, Y., Shiraiwa, M., Laskin, J., Nizkorodov, S. A., and Laskin, A.: Molecular Characterization
614   of Brown Carbon in Biomass Burning Aerosol Particles, Environ. Sci. Technol., 50, 11815-11824,
615   https://doi.org/10.1021/acs.est.6b03024, 2016.

616 Lin, P., Bluvshtein, N., Rudich, Y., Nizkorodov, S. A., Laskin, J., and Laskin, A.: Molecular Chemistry of
617   Atmospheric Brown Carbon Inferred from a Nationwide Biomass Burning Event, Environ. Sci. Technol., 51,
618   11561-11570, https://10.1021/acs.est.7b02276, 2017.

619 Lin, P., Fleming, L. T., Nizkorodov, S. A., Laskin, J., and Laskin, A.: Comprehensive Molecular Characterization of
620   Atmospheric Brown Carbon by High Resolution Mass Spectrometry with Electrospray and Atmospheric
621   Pressure Photoionization, Anal. Chem., 90, 12493-12502, https://doi.org/10.1021/acs.analchem.8b02177, 2018.

622 Liu, J., Bergin, M., Guo, H., King, L., Kotra, N., Edgerton, E., and Weber, R. J.: Size-resolved measurements of
623   brown carbon in water and methanol extracts and estimates of their contribution to ambient fine-particle light
624   absorption, Atmos. Chem. Phys., 13, 12389-12404, https://10.5194/acp-13-12389-2013, 2013.

625 Liu, J., Mo, Y., Ding, P., Li, J., Shen, C., and Zhang, G.: Dual carbon isotopes ((14)C and (13)C) and optical properties
626   of WSOC and HULIS-C during winter in Guangzhou, China, Sci. Total Environ., 633, 1571-1578,
627   https://doi.org/10.1016/j.scitotenv.2018.03.293, 2018.

628 Luciani, X., Mounier, S., Redon, R., and Bois, A.: A simple correction method of inner filter effects affecting FEEM
629   and its application to the PARAFAC decomposition, Chemom. Intell. Lab. Syst., 96, 227-238,

630   https://doi.org/10.1016/j.chemolab.2009.02.008, 2009.

631   Marrero-Ortiz, W., Hu, M., Du, Z., Ji, Y., Wang, Y., Guo, S., Lin, Y., Gomez-Hermandez, M., Peng, J., Li, Y., Secrest,
632   J., Levy Zamora, M., Wang, Y., An, T., and Zhang, R.: Formation and optical properties of brown carbon from
633   small alpha-dicarbonyls and amines, Environ. Sci. Technol., https://10.1021/acs.est.8b03995, 2018.

634   Matos, J. T. V., Freire, S. M. S. C., Duarte, R. M. B. O., and Duarte, A. C.: Natural organic matter in urban aerosols:
635   Comparison between water and alkaline soluble components using excitation–emission matrix fluorescence
636   spectroscopy and multiway data analysis, Atmos. Environ., 102, 1-10,
637   https://doi.org/10.1016/j.atmosenv.2014.11.042, 2015.

638   Mcknight, D. M., Boyer, E. W., Westerhoff, P., Doran, P. T., Kulbe, T., and Andersen, D. T.: Spectrofluorometric
639   characterization of dissolved organic matter for indication of precursor organic material and aromaticity, Limnol.
640   Oceanogr., 46, 38-48, https://doi.org/10.4319/lo.2001.46.1.0038, 2001.

641   Mo, Y., Li, J., Jiang, B., Su, T., Geng, X., Liu, J., Jiang, H., Shen, C., Ding, P., Zhong, G., Cheng, Z., Liao, Y., Tian,
642   C., Chen, Y., and Zhang, G.: Sources, compositions, and optical properties of humic-like substances in Beijing
643   during the 2014 APEC summit: Results from dual carbon isotope and Fourier-transform ion cyclotron resonance
644   mass spectrometry analyses, Environ. Pollut., 239, 322-331, https://doi.org/10.1016/j.envpol.2018.04.041, 2018.

645   Mo, Y. Z., Li, J., Liu, J. W., Zhong, G. C., Cheng, Z. N., Tian, C. G., Chen, Y. J., and Zhang, G.: The influence of
646   solvent and pH on determination of the light absorption properties of water-soluble brown carbon, Atmos.
647   Environ., 161, 90-98, https://10.1016/j.atmosenv.2017.04.037, 2017.

648   Mounier, S., Patel, N., Quilici, L., Benaim, J. Y., and Benamou, C.: Fluorescence 3D de la matière organique dissoute
649   du fleuve amazone: (Three-dimensional fluorescence of the dissolved organic carbon in the Amazon river),
650   Water Res., 33, 1523-1533, https://doi.org/10.1016/S0043-1354(98)00347-9, 1999.

651   Murphy, K. R., Butler, K. D., Spencer, R. G., Stedmon, C. A., Boehme, J. R., and Aiken, G. R.: Measurement of
652   dissolved organic matter fluorescence in aquatic environments: an interlaboratory comparison, Environ. Sci.
653   Technol., 44, 9405-9412, https://doi.org/10.1021/es102362t, 2010.

654   Murphy, K. R., Stedmon, C. A., Graeber, D., and Bro, R.: Fluorescence spectroscopy and multi-way techniques.
655   PARAFAC, Anal. Methods, 5, 6557-6566, https://doi.org/10.1039/c3ay41160e, 2013.

656   Murphy, K. R., Timko, S. A., Gonsior, M., Powers, L. C., Wunsch, U. J., and Stedmon, C. A.: Photochemistry
657   Illuminates Ubiquitous Organic Matter Fluorescence Spectra, Environ. Sci. Technol., 52, 11243-11250,
658   https://10.1021/acs.est.8b02648, 2018.

659   Park, S. S., and Yu, J.: Chemical and light absorption properties of humic-like substances from biomass burning
660   emissions under controlled combustion experiments, Atmos. Environ., 136, 114-122,
661   https://doi.org/10.1016/j.atmosenv.2016.04.022, 2016.

662   Permadi, D. A., Kim Oanh, N. T., and Vautard, R.: Assessment of emission scenarios for 2030 and impacts of black
663   carbon emission reduction measures on air quality and radiative forcing in Southeast Asia, Atmos. Chem. Phys.,
664   18, 3321-3334, https://10.5194/acp-18-3321-2018, 2018.

665   Pohlker, C., Huffman, J. A., and Poschl, U.: Autofluorescence of atmospheric bioaerosols – fluorescent biomolecules
666   and potential interferences, Atmos. Meas. Tech., 5, 37-71, https://10.5194/amt-5-37-2012, 2012.

667   Qin, J., Zhang, L., Zhou, X., Duan, J., Mu, S., Xiao, K., Hu, J., and Tan, J.: Fluorescence fingerprinting properties

668   for exploring water-soluble organic compounds in PM$_{2.5}$ in an industrial city of northwest China, Atmos.
669   Environ., 184, 203-211, https://doi.org/10.1016/j.atmosenv.2018.04.049, 2018.
670 Ramanathan, V., Li, F., Ramana, M. V., Praveen, P. S., Kim, D., Corrigan, C. E., Van Nguyen, H., Stone, E. A.,
671   Schauer, J. J., and Carmichael, G. R.: Atmospheric brown clouds: Hemispherical and regional variations in long-
672   range transport, absorption, and radiative forcing, J. Geophys. Res., 112, https://10.1029/2006JD008124, 2007.
673 See, S. W., Balasubramanian, R., and Wang, W.: A study of the physical, chemical, and optical properties of ambient
674   aerosol particles in Southeast Asia during hazy and nonhazy days, J. Geophys. Res.-Atmos., 111,
675   https://10.1029/2005JD006180, 2006.
676 Shimabuku, K. K., Kennedy, A. M., Mulhern, R. E., and Summers, R. S.: Evaluating Activated Carbon Adsorption
677   of Dissolved Organic Matter and Micropollutants Using Fluorescence Spectroscopy, Environ. Sci. Technol., 51,
678   2676-2684, https://doi.org/10.1021/acs.est.6b04911, 2017.
679 Song, J., Li, M., Jiang, B., Wei, S., Fan, X., and Peng, P.: Molecular Characterization of Water-Soluble Humic like
680   Substances in Smoke Particles Emitted from Combustion of Biomass Materials and Coal Using Ultrahigh-
681   Resolution Electrospray Ionization Fourier Transform Ion Cyclotron Resonance Mass Spectrometry, Environ.
682   Sci. Technol., 52, 2575-2585, https://doi.org/10.1021/acs.est.7b06126, 2018.
683 Song, J. Z., Li, M. J., Fan, X. J., Zou, C. L., Zhu, M. B., Jiang, B., Yu, Z. Q., Jia, W. L., Liao, Y. H., and Peng, P. A.:
684   Molecular Characterization of Water- and Methanol-Soluble Organic Compounds Emitted from Residential
685   Coal Combustion Using Ultrahigh-Resolution Electrospray Ionization Fourier Transform Ion Cyclotron
686   Resonance Mass Spectrometry, Environ. Sci. Technol., 53, 13607-13617, https://10.1021/acs.est.9b04331, 2019.
687 Stedmon, C. A., and Markager, S.: Resolving the variability in dissolved organic matter fluorescence in a temperate
688   estuary and its catchment using PARAFAC analysis, Limnol. Oceanogr., 50, 686-697,
689   https://10.4319/lo.2005.50.2.0686, 2005.
690 Tang, J., Li, J., Mo, Y., Safaei Khorram, M., Chen, Y., Tang, J., Zhang, Y., Song, J., and Zhang, G.: Light absorption
691   and emissions inventory of humic-like substances from simulated rainforest biomass burning in Southeast Asia,
692   Environ. Pollut., 262, 114266, https://doi.org/10.1016/j.envpol.2020.114266, 2020a.
693 Tang, J., Li, J., Su, T., Han, Y., Mo, Y., Jiang, H., Cui, M., Jiang, B., Chen, Y., Tang, J., Song, J., Peng, P., and Zhang,
694   G.: Molecular compositions and optical properties of dissolved brown carbon in biomass burning, coal
695   combustion, and vehicle emission aerosols illuminated by excitation–emission matrix spectroscopy and Fourier
696   transform ion cyclotron resonance mass spectrometry analysis, Atmos. Chem. Phys., 20, 2513-2532,
697   https://10.5194/acp-20-2513-2020, 2020b.
698 Wang, J., Jiang, H., Jiang, H., Mo, Y., Geng, X., Li, J., Mao, S., Bualert, S., Ma, S., Li, J., and Zhang, G.: Source
699   apportionment of water-soluble oxidative potential in ambient total suspended particulate from Bangkok:
700   Biomass burning versus fossil fuel combustion, Atmos. Environ., 235, 117624,
701   https://doi.org/10.1016/j.atmosenv.2020.117624, 2020a.
702 Wang, K., Pang, Y., He, C., Li, P., Xiao, S., Sun, Y., Pan, Q., Zhang, Y., Shi, Q., and He, D.: Optical and molecular
703   signatures of dissolved organic matter in Xiangxi Bay and mainstream of Three Gorges Reservoir, China: Spatial
704   variations and environmental implications, Sci. Total Environ., 657, 1274-1284,
705   https://10.1016/j.scitotenv.2018.12.117, 2019.

706 Wang, X., Hayeck, N., Brüggemann, M., Abis, L., Riva, M., Lu, Y., Wang, B., Chen, J., George, C., and Wang, L.:
707   Chemical Characteristics and Brown Carbon Chromophores of Atmospheric Organic Aerosols Over the Yangtze
708   River Channel: A Cruise Campaign, J. Geophys. Res.-Atmos., 125, e2020JD032497,
709   https://10.1029/2020jd032497, 2020b.
710 Wong, J. P. S., Nenes, A., and Weber, R. J.: Changes in Light Absorptivity of Molecular Weight Separated Brown
711   Carbon Due to Photolytic Aging, Environ. Sci. Technol., 51, 8414-8421, https://10.1021/acs.est.7b01739, 2017.
712 Wu, C., Wang, G., Li, J., Li, J., Cao, C., Ge, S., Xie, Y., Chen, J., Li, X., Xue, G., Wang, X., Zhao, Z., and Cao, F.:
713   The characteristics of atmospheric brown carbon in Xi'an, inland China: sources, size distributions and optical
714   properties, Atmos. Chem. Phys., 20, 2017-2030, https://10.5194/acp-20-2017-2020, 2020a.
715 Wu, F. C., Evans, R. D., and Dillon, P. J.: Separation and Characterization of NOM by High-Performance Liquid
716   Chromatography and On-Line Three-Dimensional Excitation Emission Matrix Fluorescence Detection, Environ.
717   Sci. Technol., 37, 3687-3693, https://10.1021/es020244e, 2003.
718 Wu, G., Wan, X., Gao, S., Fu, P., Yin, Y., Li, G., Zhang, G., Kang, S., Ram, K., and Cong, Z.: Humic-Like Substances
719   (HULIS) in Aerosols of Central Tibetan Plateau (Nam Co, 4730 m asl): Abundance, Light Absorption Properties,
720   and Sources, Environ. Sci. Technol., 52, 7203-7211, https://10.1021/acs.est.8b01251, 2018.
721 Wu, G., Ram, K., Fu, P., Wang, W., Zhang, Y., Liu, X., Stone, E. A., Pradhan, B. B., Dangol, P. M., Panday, A. K.,
722   Wan, X., Bai, Z., Kang, S., Zhang, Q., and Cong, Z.: Water-Soluble Brown Carbon in Atmospheric Aerosols
723   from Godavari (Nepal), a Regional Representative of South Asia, Environ. Sci. Technol., 53, 3471-3479,
724   https://doi.org/10.1021/acs.est.9b00596, 2019.
725 Wu, G., Wan, X., Ram, K., Li, P., Liu, B., Yin, Y., Fu, P., Loewen, M., Gao, S., Kang, S., Kawamura, K., Wang, Y.,
726   and Cong, Z.: Light absorption, fluorescence properties and sources of brown carbon aerosols in the Southeast
727   Tibetan Plateau, Environ. Pollut., 257, 113616, https://10.1016/j.envpol.2019.113616, 2020b.
728 Wu, G., Fu, P., Ram, K., Song, J., Chen, Q., Kawamura, K., Wan, X., Kang, S., Wang, X., Laskin, A., and Cong, Z.:
729   Fluorescence characteristics of water-soluble organic carbon in atmospheric aerosol, Environ. Pollut., 268,
730   115906, https://10.1016/j.envpol.2020.115906, 2021.
731 Xie, M., Chen, X., Holder, A. L., Hays, M. D., Lewandowski, M., Offenberg, J. H., Kleindienst, T. E., Jaoui, M., and
732   Hannigan, M. P.: Light absorption of organic carbon and its sources at a southeastern U.S. location in summer,
733   Environ. Pollut., 244, 38-46, https://10.1016/j.envpol.2018.09.125, 2019.
734 Yan, C., Zheng, M., Sullivan, A. P., Bosch, C., Desyaterik, Y., Andersson, A., Li, X., Guo, X., Zhou, T., Gustafsson,
735   Ö., and Collett, J. L.: Chemical characteristics and light-absorbing property of water-soluble organic carbon in
736   Beijing: Biomass burning contributions, Atmos. Environ., 121, 4-12,
737   https://doi.org/10.1016/j.atmosenv.2015.05.005, 2015.
738 Yan, C., Zheng, M., Desyaterik, Y., Sullivan, A. P., Wu, Y., and Collett Jr., J. L.: Molecular Characterization of Water-
739   Soluble Brown Carbon Chromophores in Beijing, China, J. Geophys. Res.-Atmos., 125, e2019JD032018,
740   https://10.1029/2019jd032018, 2020.
741 Yan, G., and Kim, G.: Speciation and Sources of Brown Carbon in Precipitation at Seoul, Korea: Insights from
742   Excitation-Emission Matrix Spectroscopy and Carbon Isotopic Analysis, Environ. Sci. Technol., 51, 11580-
743   11587, https://10.1021/acs.est.7b02892, 2017.

744   Yue, S., Ren, L., Song, T., Li, L., Xie, Q., Li, W., Kang, M., Zhao, W., Wei, L., Ren, H., Sun, Y., Wang, Z., Ellam, R.
745   M., Liu, C. Q., Kawamura, K., and Fu, P.: Abundance and Diurnal Trends of Fluorescent Bioaerosols in the
746   Troposphere over Mt. Tai, China, in Spring, J. Geophys. Res.-Atmos., 124, 4158-4173,
747   https://10.1029/2018jd029486, 2019.
748   Zhou, Y., Wen, H., Liu, J., Pu, W., Chen, Q., and Wang, X.: The optical characteristics and sources of chromophoric
749   dissolved organic matter (CDOM) in seasonal snow of northwestern China, The Cryosphere, 13, 157-175,
750   https://10.5194/tc-13-157-2019, 2019.
751   Zsolnay, A., Baigar, E., Jimenez, M., Steinweg, B., and Saccomandi, F.: Differentiating with fluorescence
752   spectroscopy the sources of dissolved organic matter in soils subjected to drying, Chemosphere, 38, 45-50,
753   https://10.1016/S0045-6535(98)00166-0, 1999.
754
755
756
757